



Adsorption geometry of CN on Cu(1 1 1) and Cu(1 1 1)/O

M. Polcik^a, M. Kittel^a, J.T. Hoelt^a, R. Terborg^a, R.L. Toomes^b,
D.P. Woodruff^{b,*}

^a Fritz-Haber-Institut der Max-Planck-Gesellschaft, Faradayweg 4-6, 14195 Berlin, Germany

^b Department of Physics, University of Warwick, Coventry CV4 7AL, UK

Received 26 May 2004; accepted for publication 11 June 2004

Available online 25 June 2004

Abstract

The adsorption geometry of CN on Cu(1 1 1), both with and without predosing with oxygen, has been investigated using N K-edge near-edge X-ray absorption fine structure (NEXAFS) and C 1s and N 1s scanned-energy mode photoelectron diffraction (PhD). The NEXAFS shows clearly that adsorbed onto clean Cu(1 1 1) the C–N axis is closely parallel to the surface, but in the presence of coadsorbed oxygen the average orientation has the axis tilted by 25° away from the surface; this confirms a much earlier report of an oxygen-induced reorientation of CN on this surface based on vibrational spectroscopy. The PhD data show very weak modulations which are rather insensitive to the emission geometry, clearly implying a high degree of disorder or a local adsorption site well-removed from any position of high point group symmetry. The best-fit structure corresponds to the CN lying slightly displaced from the three-fold coordinated hollow sites but with the C and N atoms having single Cu atom nearest neighbours at distances of 1.98 ± 0.05 and 2.00 ± 0.05 Å respectively.

© 2004 Elsevier B.V. All rights reserved.

Keywords: Photoelectron diffraction; Near edge extended X-ray absorption fine structure (NEXAFS); Chemisorption; Surface structure, morphology, roughness, and topography; Copper; Cyanogen; Oxygen; Low index single crystal surfaces

1. Introduction

Studies of the adsorption of the cyanide species, CN, at metal–solution and electrode–electrolyte interfaces, using various vibrational spectroscopies, have been motivated in part by its relevance to electroplating, although this species has also been identified as a surface intermediate in the oxida-

tion of amino acids (e.g. [1]). At these solid–liquid interfaces there is a general consensus that the CN adsorbs with its molecular axis essentially perpendicular to the surface bonding through the C end (e.g. [2–5]), although in some cases there may be some tilting [6] and the extent to which this bonding is predominantly ionic or significantly covalent has been a matter of debate [5]. Adsorbed CN has also been investigated in ultra-high vacuum studies of gas–surface reactions, mainly by dissociative adsorption of cyanogen, C₂N₂; of particular practical importance in this case is the identification of a CN-containing surface intermediate in the reaction of CO with N₂ and NO

* Corresponding author. Tel.: +44-2476523378; fax: +44-2476692016.

E-mail address: d.p.woodruff@warwick.ac.uk (D.P. Woodruff).

[7–9], raising the spectre of poisonous HCN production in three-way automotive exhaust catalysts. By contrast to the solid–liquid interface studies, investigations of adsorbed CN at the solid–vacuum interface show the molecular axis to be essentially parallel to the surface.

The most complete structural studies are for CN adsorbed in ordered $c(2 \times 2)$ overlayer phases on the fcc(1 1 0) surfaces of Ni [10–12], Rh [13] and Pd [14], variously based on one or more of the techniques of scanned-energy mode photoelectron diffraction (PhD) [15], near-edge X-ray absorption fine structure (NEXAFS) and quantitative low energy electron diffraction (LEED). In all of these systems the CN lies above second layer substrate atoms with its molecular axis in the [0 0 1] azimuth such that it straggles a pair of close-packed substrate atoms rows. The C atom lies slightly lower on the surface such that this atom is three-fold coordinated to two outermost layer and one second layer substrate atoms, whereas the N atom is two-fold coordinated to adjacent outermost layer atoms. This leads to a small tilt of the C–N axis out of the surface which falls in the range 18–25° for these three different substrates. The polarisation-angle dependence of NEXAFS has also been used to determine that the orientation of the CN molecular axis on Pd(1 1 1) is tilted by 14° away from the surface [16,17]. In addition, spectroscopic data (mainly high-resolution electron energy loss spectroscopy—HREELS) has been interpreted as indicating that CN adsorbs with its molecular axis essentially parallel to the surface on Pd(1 0 0) [18,19], on Ru(0 0 0 1) [20] and on Cu(1 1 1) [21].

HREELS has also been used to study the interaction of cyanogen with Cu surfaces pre dosed with oxygen [21–23], motivated in part by interest in the formation of the surface cyanate species, NCO [24–26]. A particularly interesting conclusion of this work [23] is that on Cu(1 1 1) pre dosing of oxygen to an estimated coverage of 0.1 ML did not lead to the formation of a surface cyanate, but a strong enhancement of the intensity of the C–N stretching band in the HREELS was taken to infer that the molecular axis of the adsorbed CN was now much more nearly perpendicular to the surface. While there appear to be no relevant calculations for the Cu(1 1 1) surface, it is interesting to

note that ab initio calculations of CN on Ni(1 0 0) have found that while there is almost no energetic difference between perpendicular and parallel orientations of the C–N axis on the clean surface, in the presence of coadsorbed O atoms the end-on perpendicular geometry is strongly favoured [27].

Here we report on the application of quantitative structural methods to investigate the behaviour of CN on Cu(1 1 1). In particular, N K-edge NEXAFS has been used to gain quantitative information on the average orientation of the surface CN species on Cu(1 1 1) with and without preadsorbed oxygen. We have also measured extensive C 1s and N 1s PhD spectra in order to try to establish the local adsorption sites.

2. Experimental details

The experiments were conducted using synchrotron radiation from the HE-TGM monochromator [28] on the BESSY electron storage ring in Berlin, in a surface science end-station equipped with the usual facilities for in situ sample preparation and characterisation. The Cu(1 1 1) sample was prepared in situ by argon ion bombardment and annealing to produce a clean and well-ordered surface as judged by soft X-ray core level photoelectron spectra and the low energy electron diffraction (LEED) pattern. The CN-covered surface was produced by a nominal saturation exposure ($200\text{--}400 \times 10^{-6}$ mbar s) of cyanogen gas produced by heating carefully-outgassed AgCN to a nominal temperature of 360 °C. The coadsorption experiments were performed by first exposing the Cu surface to $60\text{--}100 \times 10^{-6}$ mbar s oxygen followed by similar $150\text{--}300 \times 10^{-6}$ mbar s exposures of cyanogen; these conditions were chosen to reproduce those used in the earlier HREELS study of this system [21–23]. Photoemission spectra were recorded using a 152 mm mean radius spherical-sector electrostatic analyser (VG Scientific) equipped with three-channeltron parallel detection. This analyser was mounted at 60° relative to the incident synchrotron radiation, and has an acceptance angle of $\pm 4.5^\circ$. We have found that this acceptance angle appears to be around optimal for PhD determinations of local adsorbate structure.

Much smaller acceptance angles greatly reduce the measured intensity and make the computational simulations very time-consuming (see below), whereas much larger acceptance angles ‘wash out’ the PhD modulations. By comparison with photoemission spectra taken previously with the same instrumentation for the 0.5 ML coverage phases of O on N on Cu(100), we estimate that the adsorbate coverages studied in the present experiments were: pure CN, 0.28 ML; coadsorbed O and CN, O coverage 0.12 ML, CN 0.42 ML. The precision of these estimates is probably about 10–20%.

N K-edge NEXAFS spectra were recorded by monitoring the intensity of the N KLL Auger emission for a range of different grazing incidence angles, normalised to the sample drain current as a measure of the incident beam intensity variations with photon energy. Similar measurements were made from the clean Cu(111) surface and the adsorbate spectra were normalised by dividing by these reference spectra. The PhD technique [15] exploits the coherent interference which occurs between the directly emitted component of the photoelectron wavefield resulting from the photoionisation of an adsorbate core level, and the components of this same wavefield which are elastically scattered by the surrounding atoms. The photoelectron kinetic energy, and thus the associated photoelectron wavelength, is varied by changing the photon energy, causing different scattering pathways to switch in and out of phase. This leads to modulations in the photoemission intensity as a function of energy in any specific direction. Using relatively low photoelectron energies (<500 eV), at which elastic backscattering cross-sections are reasonably large, these data provide quantitative information on the adsorbate-substrate registry. Notice that the same photoelectron diffraction effects can be monitored by measuring the intensity as a function of polar and azimuthal emission angles at fixed energies [15], but we have found the use of energy scans in fixed directions to be a more convenient way of probing the information and our experiment is designed for this purpose. In the present case PhD spectra were obtained by measuring 80 eV wide photoelectron energy distributions centred around the C and N 1s emission peaks at photoelectron energies in the

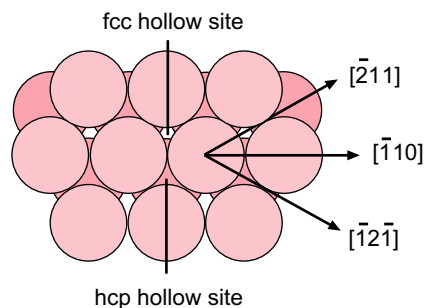


Fig. 1. Schematic plan view of the Cu(111) surface defining azimuthal directions and identifying the two inequivalent three-fold coordinated hollow sites available on this surface.

range 80–350 eV at 2 eV steps. Each of these peaks was fitted by a Gaussian peak, a Gaussian-broadened step, and a template background function to obtain a graph of the integrated 1s peak area as a function of photoelectron kinetic energy, $I(E)$. Normalisation of this gave the PhD modulation spectrum $\chi(E) = (I(E) - I_0(E))/I_0(E)$ where $I_0(E)$ is the non-diffracted intensity which is taken to be a smooth stiff spline through the experimental data. PhD modulation spectra of this type were obtained in most of the directions within the range of polar emission angles from 0° to 60° in 10° steps and in each of the three symmetrically inequivalent high symmetry azimuths, namely one of the $\langle 110 \rangle$ azimuths and two inequivalent $\langle 112 \rangle$ azimuths at $+30^\circ$ and -30° relative to $\langle 110 \rangle$ labelled here as $[\bar{2}11]$ and $[\bar{1}2\bar{1}]$ (at $+30^\circ$ and -30° to $[\bar{1}10]$)—see Fig. 1).

3. Results and data analysis

3.1. NEXAFS

Fig. 2 shows a summary of the N K-edge NEXAFS spectra from the pure CN and CN/O coadsorption surfaces for several different incidence angles; in the standard NEXAFS nomenclature the angles shown are the grazing incidence angles (i.e. normal incidence corresponds to 90°) but this angle also corresponds to the angle, θ_E , between the electric vector of the incident plane-polarised radiation and the surface normal.

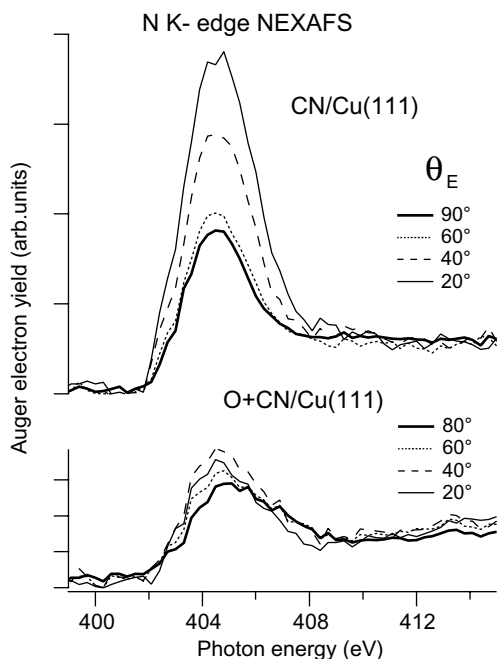


Fig. 2. N K-edge NEXAFS spectra for CN on Cu(111) with and without coadsorbed O recorded at several different grazing incidence angles, θ_E .

Clearly there is a significant difference induced by the preadsorbed oxygen. For the pure CN layer the single NEXAFS peak close to threshold, associated with excitation into the unoccupied π -resonance, increases in intensity by about a factor of two as the grazing incidence angle is decreased. By contrast, with preadsorbed oxygen this variation in intensity is much weaker. This intensity variation provides a basis for determining the average tilt angle of the molecular axis away from the surface normal, β . To this end we exploit the dependence of the NEXAFS intensity on the angle, δ , between the electric vector of the incident radiation and the final state π -orbital (i.e. the direction perpendicular to the molecular axis in the plane in which the π -orbital is symmetric) which is given by $\cos^2 \delta$ [29]. For a molecular axis tilted relative to the surface normal there are formally two non-degenerate π -orbitals, one lying within the plane of tilt and the other perpendicular to this plane, and we here assume that these two final states contribute equally to the observed π -reso-

nance in which the two contributions are unresolved. In this case, for perfectly plane-polarised incident radiation, after averaging over all equivalent azimuths on the three-fold symmetric surface, the NEXAFS intensity variation is given by $I \propto \sin^2 \theta_E (1 + \cos^2 \beta) + 2 \sin^2 \beta \cos^2 \theta_E$.

By simple fitting of the NEXAFS π -resonance peak to a Gaussian profile one can extract the polarisation-angle dependence of the amplitude of this feature in a more quantitative fashion (Fig. 3) and compare this with the predicted dependence for different tilt angles. Fig. 3 shows the best-fit theory curves obtained for values of the tilt angle, β , of 90° for the pure CN layer and 65° for the CN with preadsorbed oxygen. These theoretical curves assumed that the incident radiation was 90% horizontally polarised and 10% vertically polarised. Other measurements of the polarisation of the output flux from the HE-TGM beamline indicate a polarisation as high as 96%, but using this figure gave essentially identical (within less than 1°) optimum tilt angles. We therefore conclude that for the pure CN layer the C–N axis is exactly parallel to the surface (to within the esti-

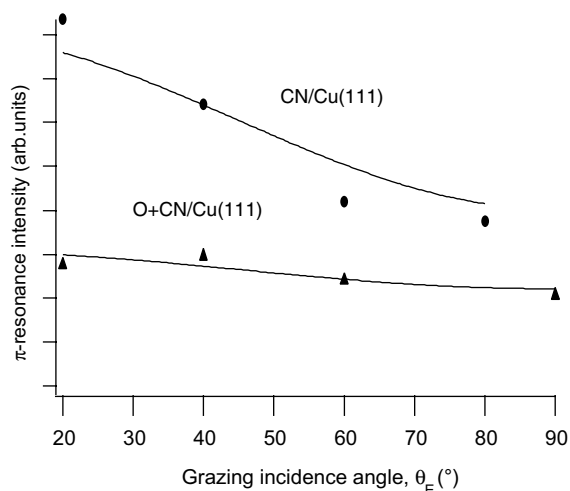


Fig. 3. Dependence of the N K-edge NEXAFS π -resonance peak intensity from CN on Cu(111) as a function of the grazing incidence (and polarisation) angle, θ_E , extracted from the spectra of Fig. 2. The full lines are theoretical fits corresponding to tilt angle of the C–N axis relative to the surface normal of 90° for the pure CN layer and 65° with preadsorbed O.

mated precision of $\pm 15^\circ$) and with preadsorbed oxygen the *average* tilt angle of the C–N axis is 25° from parallel to the surface. We should stress that because the oxygen precoverage is relatively low (0.12 ML) and the range of interaction of the CN and O is unknown, it is possible that on the oxygen precovered surfaces the NEXAFS measurements represent an average over some CN molecules which are parallel to the surface which is locally devoid of oxygen while others, influenced by the preadsorbed oxygen, are more strongly tilted to the surface.

3.2. PhD

Fig. 4 shows an overview of the C 1s and N 1s PhD modulation spectra obtained from the pure CN layer on Cu(1 1 1). The most striking feature of these data is that the modulations are in all cases very weak. A few spectra show consistent modulations in excess of $\pm 10\%$, but in many cases the modulations are only of order 5% or less. A necessary consequence of this is that the signal-to-noise ratio is also rather poor. Based on previous studies of a very large number of atomic and molecular adsorbate systems (many on Cu(1 1 1))

we have found that for adsorption in a high symmetry site the PhD modulations seen in a direction corresponding to a near- 180° nearest-neighbour backscattering direction are typically of order ± 30 – 40% , with values as large as $\pm 80\%$ in a few cases. By contrast, weak modulation can result from the emitter atoms being well-removed from such high symmetry sites, because the experiment then averages (sums incoherently) over all the symmetrically equivalent local domains of the adsorbate on the surface; in this case, a favoured 180° backscattering direction for one domain (which should give strong modulations) will not correspond to such a favourable geometry for the many other symmetrically equivalent domains which will contribute only weak modulations of different periodicities. A similar situation, of course, can also arise if multiple (symmetrically inequivalent) adsorption sites are co-occupied. A further feature of the data which indicates low symmetry or multiple sites are occupied is the generally weak dependence of the PhD spectra on the azimuth of measurement, clearly seen in Fig. 4.

Our standard procedure for extracting the structure from a PhD data set contains two ingredients. In the first stage we generally apply

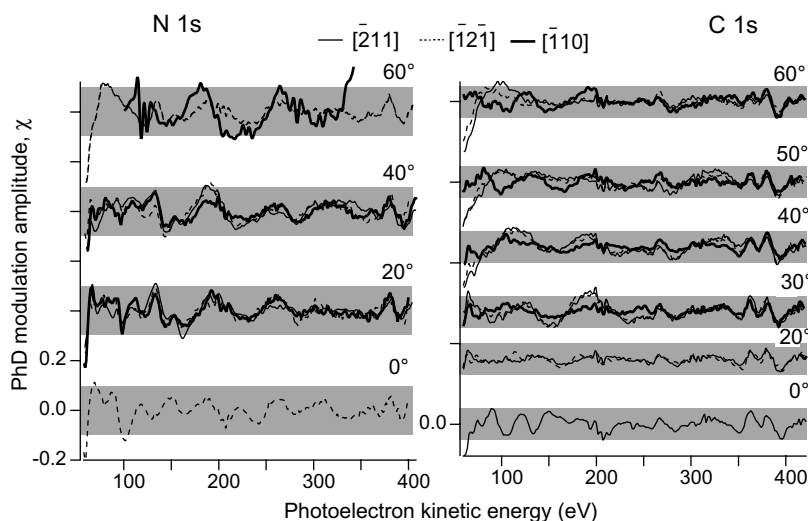


Fig. 4. Overview of the N 1s and C 1s PhD spectra recorded from the pure CN on Cu(1 1 1) at different polar emission angles and in different azimuthal planes (see Fig. 1). The shaded regions correspond to the modulation range $\pm 10\%$, providing a clear indication of the weakness of the modulations.

the ‘projection method’ of direct data inversion [30,31] to obtain an approximate ‘image’ of the scattering atoms around the emitter. This method, however, relies on the data set containing strong modulations in directions corresponding to near-180° nearest neighbour backscattering directions as is obtained from highly symmetric adsorption sites. For emitter sites well-removed from such high symmetry locations these clear emitter-neighbour directions cannot be identified due to domain averaging and the method fails to identify near-neighbour scatterer locations in a convincing fashion [32]. In the present case we must therefore rely entirely on what is normally the second stage of trial-and-error modelling, simulating the experimental data with multiple scattering calculations for different trial structures. These calculations are performed with codes developed by Fritzsche [33–35] which are based on the expansion of the final state wave-function into a sum over all scattering pathways which the electron can take from the emitter atom to the detector outside the sample. A magnetic quantum number expansion of the free electron propagator is used to calculate the scattering contribution of an individual scattering path. Double and higher order scattering events are treated by means of the reduced angular momentum expansion (RAME). The finite energy resolution and angular acceptance of the electron energy analyser are accounted for analytically; both of these instrumental effects reduce the importance of more distant scatterers and thus allow convergence of the calculations with less scattering paths. Anisotropic vibrations for the emitter atom and isotropic vibrations for the scattering atoms are also taken into account. The comparison between theoretical and experimental modulation amplitudes, χ_{th} and χ_{ex} , is quantified by the use of a reliability factor

$$R_m = \frac{\sum (\chi_{\text{th}} - \chi_{\text{ex}})^2}{\sum (\chi_{\text{th}}^2 + \chi_{\text{ex}}^2)}$$

where a value of 0 corresponds to perfect agreement, a value of 1 to uncorrelated data, and a value of 2 to anti-correlated data. The search in parameter space to locate the structure having the minimum R -factor was performed with the help of an adapted Newton–Gauss algorithm. In order to

estimate the errors associated with the individual structural parameters we use an approach based on that of Pendry which was derived for LEED [36]. This involves defining a variance in the minimum of the R -factor, R_{min} as

$$\text{Var}(R_{\text{min}}) = R_{\text{min}} \sqrt{2/N}$$

where N is the number of ‘independent pieces of structural information’ contained in the set of modulation functions used in the analysis. All parameter values giving structures with R -factors less than $R_{\text{min}} + \text{Var}(R_{\text{min}})$ are regarded as falling within one standard deviation of the ‘best-fit’ structure. More details of this approach, in particular on the definition of N , can be found elsewhere [37].

A particular problem in establishing the correct structure in the present case arises from the very weak PhD modulations and the associated implication that both the C and N emitter atoms are well-removed from any high symmetry adsorption site. Weak modulations imply poor signal-to-noise ratios which ensure that even for a correct structure the R -factor will be relatively large, making this parameter less sensitive to subtle changes in the adsorption geometry. Domain averaging over symmetrically equivalent low symmetry adsorption sites also leads to a relatively weak dependence of the theoretical PhD modulation spectra on the exact geometry. We may therefore anticipate that the precision with which we can locate the adsorption geometry will be relatively low. Initial attempts to determine the local adsorption sites of the C and N atoms independently, using six or more selected PhD spectra from each emitter confirmed the fact that no adsorption geometries close to high symmetry sites yielded even plausible fits to the experimental spectra. Moreover, including experimental PhD spectra with very weak modulations was counter-productive, because the R -factors for these individual spectra were always large and simply lowered the sensitivity of the global (multi-spectral) R -factor to structural changes. The final structural optimisation was therefore performed by simultaneously optimising the fit to a smaller subset of both C 1s and N 1s PhD spectra which showed the strongest modulations, applying the constraint that the C–N

distance was always 1.09 Å and that the C–N axis is closely parallel to the surface as indicated by the NEXAFS results. Additional tests allowing the C–N axis to tilt slightly yielded no improvement in the fit to the PhD spectra, although similar checks on the influence of the assumed C–N distance found that the lowest *R*-factor was found with a bondlength of only 1.00 Å. While the true value of this intramolecular bondlength is not known, in molecules the C≡N bond is typically 1.16 Å [38] while adsorbed on Ni(110) values of 1.25 ± 0.12 Å [10] and 1.17 ± 0.08 Å [12] have been found. We therefore regard the value of 1.00 Å as improbably short and give the results for the somewhat larger value of 1.09 Å. Notice, though, that the optimal coordinates of the N and C atoms found using C–N bondlengths constrained in the range 1.00–1.20 Å all fell within the estimated precision of these values for the value of 1.09 Å.

The best-fit simulated spectra are compared with the corresponding experimental spectra in Fig. 5. The overall *R*-factor value is 0.33 and reflects the moderately good agreement in all the main modulations. For systems showing stronger modulations we have generally found the mini-

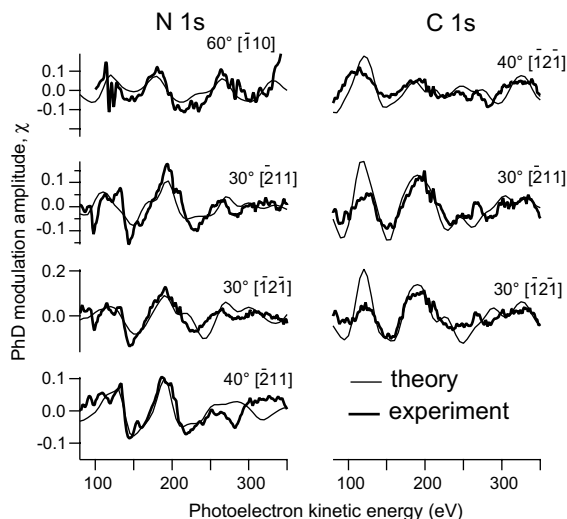


Fig. 5. Comparison of a subset of the N 1s and C 1s PhD experimental modulation spectra (Fig. 3) recorded from the pure CN layer on Cu(111) with the results of the theoretical multiple scattering simulations for the best-fit adsorption geometry (see Fig. 6).

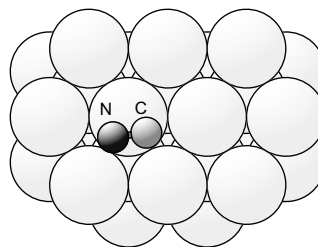


Fig. 6. Schematic plan view of the Cu(111) surface (the Cu atoms shown as large lightly-shaded spheres) with CN adsorbed in the geometry leading to the best-fit to the experimental PhD spectra (Fig. 5).

mum achievable *R*-factor is less than 0.3, and indeed in some cases less than 0.2, but in the present case of weak modulations the value of 0.33 is actually rather encouraging. Fig. 6 shows a schematic diagram of the geometry corresponding to these best-fit PhD spectra. The C and N atoms are in sites offset from atop towards bridging sites on the Cu(111) surface such that one Cu atom is very significantly closer to both the C and N atom (1.98 ± 0.05 and 2.00 ± 0.05 Å respectively) than the next-nearest neighbour Cu atoms (2.58 and 2.51 Å). The molecule is 1.82 ± 0.04 Å above the outermost Cu layer of a bulk-terminated substrate; no significant improvement in the fit resulted from allowing relaxation of the substrate. The precision in the lateral positions of the atoms on the surface was found to be ± 0.09 Å, although the optimised fit yielded an anomalously large optimum value of the root-mean-square vibrational amplitude of the C atoms ($0.37(+0.60/-0.25)$ Å) which may reflect significant static disorder in this position. Notice that the centre of the molecule occupies a site roughly midway between atop and a three-fold coordinated hollow. There are, of course, two inequivalent hollow sites on a fcc(111) surface, one above a second layer substrate atom ('hcp hollow') and one above a third layer substrate ('fcc hollow') (Fig. 1). Our calculations indicate that these two sites are occupied with equal probability.

In the case of CN adsorbed onto the Cu(111) surface preadsorbed with oxygen, Fig. 7 shows a comparison of C 1s and N 1s PhD spectra recorded from the surface compared with comparable data from the pure CN layer. Clearly the PhD spectra from the two phases are very similar;

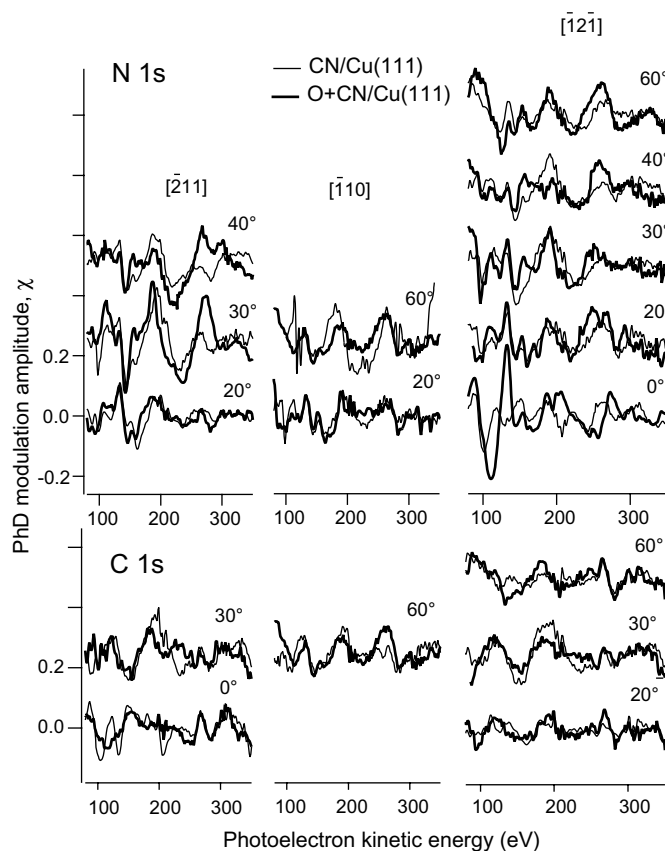


Fig. 7. Overview of the N 1s and C 1s PhD spectra recorded from CN adsorbed on Cu(111) with and without preadsorbed O.

there are certainly detailed differences, but these are not very systematic. For example, for the N 1s spectra recorded at 30° and 40° polar emission angle in the $[\bar{2}11]$ azimuth the modulations are somewhat stronger with the preadsorbed O than without, but the contrary is true in the equivalent spectra in the $[\bar{1}2\bar{1}]$ azimuth. Similar effects are seen in the C 1s PhD spectra. As the NEXAFS clearly indicates a change in the orientation of the C–N axis away from parallel to the surface, one might have expected that the molecule would now be bonded to the surface through only one end and that the atom at the other end, no longer directly bonding to the Cu and thus more distant from the Cu scatterers, would lead to significantly weaker PhD modulations. No such systematic behaviour can be discerned for either emitter atom. Of course, the role of the coadsorbed O is far from

clear. Chemisorbed oxygen on Cu(111) does not form any long-range ordered structures, but at high coverage there is clear evidence from several different techniques for restructuring of the outermost Cu atom layer(s), possibly to form a local pseudo-(100) reconstruction (see [39] and references therein). At lower coverages even less is known about the structure of O on Cu(111), but it is certainly possible that similar reconstruction occurs locally. In this case it may be inappropriate to think of the CN adopting a slightly modified geometry on the Cu(111) surface, because the reconstruction may produce a far more atomically rough surface on which a tilted molecule might still bond to the surface Cu atoms through both the C and N atoms (as has been found for the similarly weakly tilted CN species on several fcc(110) surfaces [10–14]). On the other hand, if

the interaction between the adsorbed O and CN species is highly local, it is possible that some fraction of the CN molecules are far more strongly tilted out of the surface plane through interaction with the O atoms, while the remainder (perhaps the majority) retain the geometry on the clean surface.

4. Conclusions

N K-edge NEXAFS studies of CN and CN/O coadsorption on Cu(111) confirm earlier qualitative results from HREELS that the oxygen coadsorption causes the C–N axis to tilt up out of the surface plane, and provides some quantification of these conclusions. Specifically, in the absence of coadsorbed O the molecular axis of the adsorbed CN is parallel to the surface to within the limits of precision ($\pm 15^\circ$) whereas in the presence of coadsorbed O the axis is tilted by an average angle of $25 \pm 15^\circ$ away from parallel to the surface. Note that we estimate the coverages of O and CN in the coadsorption phase to be 0.12 and 0.42 ML respectively, so it is possible that this tilt angle represents an average over two distinct values with CN unaffected by O remaining parallel to the surface while the second species associated with the O is more nearly perpendicular to the surface. C 1s and N 1s scanned-energy mode photoelectron diffraction from the pure CN layer show very weak modulations characteristic of a low symmetry adsorption site or multiple sites. Constraining the C–N bond length and bond orientation (the latter from the NEXAFS results) we find the best-fit structure corresponds to the molecule occupying an off-atop geometry with both C and N atoms having a single nearest-neighbour Cu atom at distances of 1.98 ± 0.05 and 2.00 ± 0.05 Å respectively.

Acknowledgements

This work was supported by the European Community through Large Scale Facilities support to BESSY, and by the Physical Sciences and Engineering Research Council (UK) in the form of

a research grant and a Senior Research Fellowship for DPW.

References

- [1] F. Huerta, E. Morallón, F. Cases, A. Rodes, J.L. Vázquez, A. Aldaz, *J. Electroanal. Chem.* 431 (1997) 269.
- [2] R.E. Benner, K.U. von Raben, R. Dornhaus, R.K. Chang, B.L. Laube, F.A. Otter, *Surf. Sci.* 102 (1981) 7.
- [3] K. Kunimatsu, H. Seki, W.G. Golden, J.G. Gordon II, M.R. Philpott, *Surf. Sci.* 158 (1985) 596.
- [4] D.S. Corrigan, P. Gao, L.-W.H. Leung, M.J. Weaver, *Langmuir* 2 (1986) 744.
- [5] W. Daum, F. Dederichs, J.E. Müller, *Phys. Rev. Lett.* 80 (1998) 766 (erratum *Phys. Rev. Lett.* 85 (2000) 2655).
- [6] B. Ren, X.-Q. Li, D.-Y. Wu, J.-L. Yao, Y. Xie, Z.-Q. Tian, *Chem. Phys. Lett.* 322 (2000) 561.
- [7] P. Jakob, *Chem. Phys. Lett.* 263 (1996) 607.
- [8] D.R. Mullins, Lj. Kundakovic, S.H. Overbury, *J. Catal.* 195 (2000) 169.
- [9] J.H. Miners, A.M. Bradshaw, P. Gardner, *Phys. Chem. Chem. Phys.* 1 (1999) 4909.
- [10] N.A. Booth et al., *Surf. Sci.* 416 (1998) 448.
- [11] D. Brown, D.P. Woodruff, T.C.Q. Noakes, P. Bailey, *Surf. Sci.* 476 (2001) L241.
- [12] C. Bittencourt, E.A. Soares, D.P. Woodruff, *Surf. Sci.* 526 (2003) 33.
- [13] F. Bondino, A. Baraldi, H. Over, G. Comelli, P. Lacovig, S. Lizzit, G. Paolucci, R. Rosei, *Phys. Rev. B* 64 (2001) 085422.
- [14] F. Bondino, E. Vesselli, A. Baraldi, G. Comelli, A. Verdini, A. Cossaro, L. Floreano, A. Morgante, *J. Chem. Phys.* 118 (2003) 10735.
- [15] D.P. Woodruff, A.M. Bradshaw, *Rep. Prog. Phys.* 57 (1994) 1029.
- [16] J. Somers, M.E. Kordesch, T. Lindner, H. Conrad, A.M. Bradshaw, G.P. Williams, *Surf. Sci.* 188 (1987) L693.
- [17] M.E. Kordesch, T. Lindner, J. Somers, W. Stenzel, H. Conrad, A.M. Bradshaw, G.P. Williams, *Spectrochim. Acta* 43A (1987) 1561.
- [18] K. Besenthal, G. Chiarello, M.E. Kordesch, H. Conrad, *Surf. Sci.* 178 (1986) 667.
- [19] M.E. Kordesch, W. Stenzel, H. Conrad, *Surf. Sci.* 186 (1987) 601.
- [20] W.H. Wienberg, D.F. Johnson, Y.-Q. Wang, J.E. Parmeter, M.M. Hills, *Surf. Sci.* 235 (1990) L299.
- [21] M.E. Kordesch, W. Feng, W. Stenzel, M. Weaver, H. Conrad, *J. Electron. Spectrosc. Relat. Phenom.* 44 (1987) 149.
- [22] W. Feng, W. Stenzel, H. Conrad, M.E. Kordesch, *Surf. Sci.* 211/212 (1989) 1044.
- [23] M.E. Kordesch, W. Stenzel, H. Conrad, M.J. Weaver, *J. Am. Chem. Soc.* 109 (1987) 1878.
- [24] D.A. Outka, S.W. Jorgensen, C.M. Friend, R.J. Madix, *J. Mol. Catal.* 21 (1983) 375.

- [25] H. Celio, K. Mudalige, P. Mills, M. Trenary, *Surf. Sci.* 394 (1997) L168.
- [26] A.F. Carley, M. Chinn, C.R. Parkinson, *Surf. Sci.* 537 (2003) 64.
- [27] H. Yang, J.L. Whitten, *J. Chem. Phys.* 107 (1997) 8518.
- [28] E. Dietz, W. Braun, A.M. Bradshaw, R.L. Johnson, *Nucl. Instrum. Methods Phys. Res. A* 239 (1985) 359.
- [29] J. Stöhr, R. Jaeger, *Phys. Rev. B* 26 (1982) 4111.
- [30] Ph. Hofmann, K.-M. Schindler, *Phys. Rev. B* 47 (1993) 13941.
- [31] Ph. Hofmann, K.-M. Schindler, S. Bao, A.M. Bradshaw, D.P. Woodruff, *Nature* 368 (1994) 131.
- [32] D.P. Woodruff, P. Baumgärtel, J.T. Hoefl, M. Kittel, M. Polcik, *J. Phys.: Condens. Matter* 13 (2001) 10625.
- [33] V. Fritzsche, *J. Phys.: Condens. Matter* 2 (1990) 1413.
- [34] V. Fritzsche, *Surf. Sci.* 265 (1992) 187.
- [35] V. Fritzsche, *Surf. Sci.* 213 (1989) 648.
- [36] J.B. Pendry, *J. Phys. C: Solid State Phys.* 13 (1980) 937.
- [37] N.A. Booth et al., *Surf. Sci.* 387 (1997) 152.
- [38] R.C. Weast (Ed.), *CRC Handbook of Chemistry and Physics*, 58th edition, CRC Press, West Palm Beach, USA, 1977.
- [39] R.L. Toomes, D.P. Woodruff, M. Polcik, S. Bao, Ph. Hofmann, K.-M. Schindler, A.M. Bradshaw, *Surf. Sci.* 445 (2000) 300.